

Engineering two-dimensional materials from single-layer NbS₂

Timo Knispel,[†] Daniela Mohrenstecher,[†] Carsten Speckmann,[†] Affan Safeer,[†] Camiel van Efferen,[†] Virgínia Boix,[‡] Alexander Grüneis,[†] Wouter Jolie,[†] Alexei Preobrajenski,[¶] Jan Knudsen,[‡] Nicolae Atodiresei,[§] Thomas Michely,[†] and Jeison Fischer^{*,†}

[†]*II. Physikalisches Institut, Universität zu Köln, Zùlpicher Straße 77, D-50937 Cologne, Germany*

[‡]*NanoLund and Division of Synchrotron Radiation Research, Department of Physics, Lund University, SE-22100 Lund, Sweden*

[¶]*MAX IV Laboratory, Lund University, SE-221 00 Lund, Sweden*

[§]*Peter Grünberg Institut (PG-1), Forschungszentrum Jùlich, Wilhelm-Johnen-StraÙe, D-52428 Jùlich, Germany*

E-mail: jfischer@ph2.uni-koeln.de

Abstract

Starting from a single layer of NbS₂ grown on graphene by molecular beam epitaxy, the single unit cell thick 2D materials Nb_{5/3}S₃-2D and Nb₂S₃-2D are created using two different pathways. Either annealing under sulfur-deficient conditions at progressively higher temperatures or deposition of increasing amounts of Nb at elevated temperature result in phase-pure Nb_{5/3}S₃-2D followed by Nb₂S₃-2D. The materials are characterized by scanning tunneling microscopy, scanning tunneling spectroscopy and X-ray photoemission spectroscopy. The experimental assessment combined with systematic density functional theory calculations reveals their structure. The 2D materials are covalently bound without any van der Waals gap. Their stacking sequence and structure are at variance with expectations based on corresponding bulk materials highlighting the importance of surface and interface effects in structure formation.

Keywords: niobium disulfide, single layer, molecular beam-epitaxy, covalent transformation

Thinning down a layered material to few or single layers transforms it into a two-dimensional (2D) material. The typical way of obtaining a 2D material is by exfoliation of the bulk crystal. The method is simple, the structural quality of exfoliated layers is generally very good,^{1,2} stacking of layers to create vertical heterostructures with new functions is straightforward,^{3,4} and finally twisted stacking opened the door for moiré physics.⁵

Nevertheless, exfoliation as a method has several significant limitations. Beyond its fundamental scalability issues, exfoliation is ineffective in preparing single or few-layer thick 2D materials from covalently bound bulk crystals. Such crystals lack van der Waals gaps and, consequently, cannot be adequately exfoliated. Additionally, exfoliation cannot be used for synthetically constructed 2D materials that have no bulk counterparts in terms of structure or composition.

The scope of 2D materials can be substantially broadened by the use of growth methods like molecular beam epitaxy (MBE) or chemical vapor deposition (CVD). For example, provision of more than one metal during growth enables one to explore the entire composition space between two dissimilar transition metal dichalcogenides (TMDCs) on the single layer level⁶ or to create vertical TMDC heterostructures with continuously tunable moiré periodicity by using the composition dependent lattice parameters.⁷ Variation of the metal chemical potential enables the production of thin films across the entire sequence of self-intercalation compounds known from bulk crystals, allowing for the discovery of magnetic order in some of these intercalated phases.⁸

Annealing an initial transition metal chalcogenide with or without chalcogene flux, possibly following prior metal deposition, is another strategy applied to create new phases. Examples are the annealing-induced single-layer transformations of CrSe_2 into Cr_2Se_3 ,⁹ of VS_2 into stripped V_2S_3 ¹⁰ or V_4S_7 ,¹¹ of PtTe_2 into Pt_2Te_2 ,¹² of $\alpha\text{-FeSe}$ into kagome Fe_5S_8 ,¹³ or of Bi_2Se_3 into MnBi_3Se_4 .¹⁴ The enumeration is by far not complete.

In the present manuscript we investigate

phase transitions of single-layer NbS_2 . This TMDC has attracted substantial research interest due to its superconductivity in the bulk^{15–17} and its charge-density wave in the single layer.^{18,19} Moreover, self-intercalated $\text{Nb}_{1+x}\text{S}_2$ is an excellent catalyst for the hydrogen evolution reaction.²⁰

Besides the van der Waals material NbS_2 , the Nb-S phase diagram displays a zoo of phases without van der Waals gap, *i.e.*, being covalently bound, of which the structures were carefully investigated by X-ray diffraction.^{21,22} Whether any of these covalently bound bulk phases possesses a 2D pendant is still unexplored. Here we establish and characterize two Nb_xS_y -2D compounds of single unit cell thickness, namely $\text{Nb}_{5/3}\text{S}_3$ -2D and Nb_2S_3 -2D. To avoid confusion with bulk materials with the same composition, but different structure, "-2D" is attached to the stoichiometric formulas indicating the yet undescribed 2D materials. Due to their single unit cell thickness, these compounds are referred to as single-layer materials. A single layer consists of stacked S-Nb-S-Nb-S planes of atoms. Starting from MBE-grown single-layer NbS_2 , the new phases are established under ultrahigh vacuum conditions via two different kinetic pathways, either through pure annealing or by metal deposition at elevated temperature. We find that each phase can be prepared phase-pure, making its investigation by averaging techniques feasible.

Beyond our methodology for creating these materials, we highlight three important findings that are of broader relevance and can be generalized to the covalent growth of other layered 2D materials. Firstly, applying careful titration based on a well calibrated evaporator is an efficient tool to determine the stoichiometry of an unknown compound resulting from phase transformation. Secondly, the structures of the resulting 2D materials differ from the known bulk phases, although their chemical composition is rather similar. Our results, thus indicate that surface effects are important and consequently assumptions that the compounds can be described from corresponding bulk phases may fail. Thirdly, we show that the explicit inclusion of the substrate in theoretical calcu-

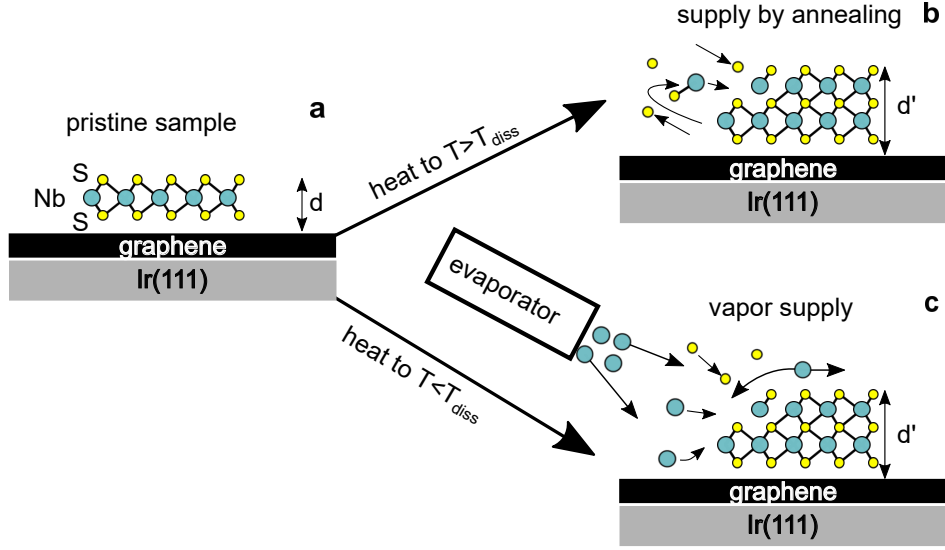


Figure 1: Concept of covalent transformation. (a) Single-layer H-NbS₂ on Gr/Ir(111). (b) Covalent transformation by heating and dissociation. (c) Covalent transformation by deposition of additional Nb.

lations is necessary to provide a valuable insight into the range of possible phases and to guide the interpretation of experiments.

Results

Concepts for covalent transformation of single-layer NbS₂

Our course of action to achieve covalent growth is exemplified for NbS₂ in Figure 1. Figure 1a displays single-layer H-NbS₂ grown on graphene (Gr) on Ir(111). The first strategy is to heat up the sample to a temperature T_{diss} that causes NbS₂ to partially dissociate [Figure 1b]. Some of the S of NbS₂ escapes into vacuum or intercalates between Gr and Ir(111). The remaining Nb excess triggers a phase transformation to a covalently bonded niobium-rich compound composed of 3 atomic planes of S separated by Nb planes. The new compound exhibits an increased height d' . Evidently, the partial dissociation of the single-layer NbS₂ of height d in combination with the larger height d' of the new phase formed without supply of additional material causes a reduction in sample coverage. The second strategy is to induce covalent growth by deposition of additional Nb at a temperature $T < T_{diss}$, see Figure 1c. When

arriving on the surface, the deposited Nb reacts with the existing NbS₂ and thereby triggers the phase transformation. In both cases identical phases can be obtained.

Covalent transformation by NbS₂ annealing

This section describes the transformation of NbS₂ into two different phases richer in Nb obtained by heating to successively higher temperatures with $T > T_{diss}$.

Figure 2a displays a scanning tunneling microscopy (STM) image of pristine single-layer NbS₂ islands grown on Gr/Ir(111) by room temperature deposition of 0.34 ML Nb in S vapor and subsequent annealing to 820 K (compare Methods). The islands cover an area fraction of 0.34, are continuous over Ir substrate steps under the Gr carpet, and are of irregular shape. The islands display an apparent height of $d = 0.62 \pm 0.01$ nm at $V_s = 1.00$ V as exemplified by the height profile below the topograph (d depends slightly on the tunneling voltage; $d = 0.58 \pm 0.01$ nm at $V_s = -1.00$ V). The measured apparent heights fit reasonably well to the apparent height of 0.578 nm reported for single-layer NbS₂ on Gr/6H-SiC(0001)¹⁸ and to half of the c-axis lattice constant of 1.195 nm of bulk

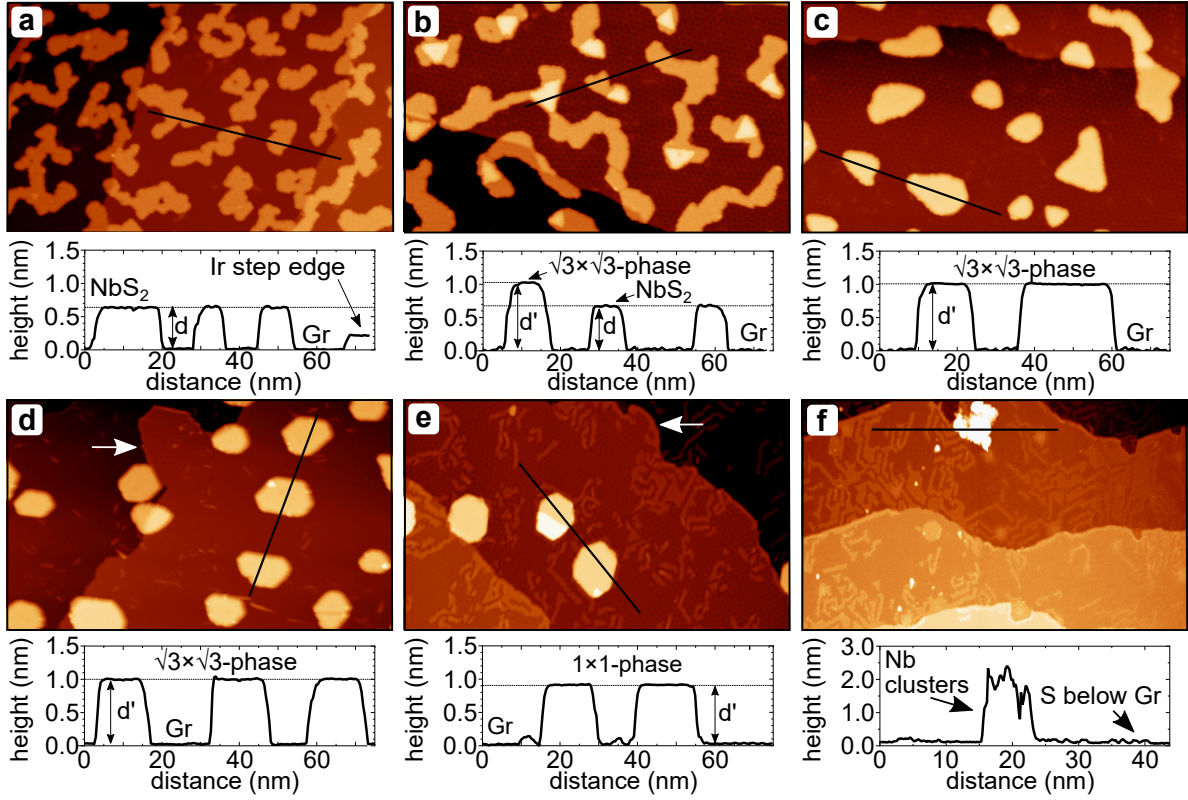


Figure 2: STM topographs of an isochronal annealing sequence of initial single-layer NbS_2 islands without supply of additional S. Annealing intervals are 360 s. (a) single-layer NbS_2 islands after room temperature growth and annealing to 820 K. (b)-(f) After additional annealing to (b) 920 K, (c) 1020 K, (d) 1120 K, (e) 1220 K, and (f) 1320 K. Height profiles along the black lines are shown below the topographs. Height levels $d = 0.62$ nm, $d' = 0.99$ nm and $d' = 0.93$ nm distinguish between single-layer NbS_2 , $\sqrt{3} \times \sqrt{3}$ - phase, 1×1 - phase, respectively. Image information: for all size $150 \text{ nm} \times 90 \text{ nm}$, a $V_s = 1.0 \text{ V}$, $I_t = 0.23 \text{ nA}$; (b) $V_s = 0.95 \text{ V}$, $I_t = 0.34 \text{ nA}$; (c) $V_s = 1.0 \text{ V}$, $I_t = 0.26 \text{ nA}$; (d) $V_s = 0.92 \text{ V}$, $I_t = 0.33 \text{ nA}$; (e) $V_s = 1.0 \text{ V}$, $I_t = 0.32 \text{ nA}$; (f) $V_s = 2.2 \text{ V}$, $I_t = 0.06 \text{ nA}$.

NbS_2 .¹⁶ In our previous work,¹⁹ it was firmly established that under these conditions NbS_2 on Gr/Ir(111) grows in the H-phase, in agreement with the findings for single-layer NbS_2 on Au(111)²³ and bulk NbS_2 .¹⁶

While NbS_2 islands are stable at 820 K independent of the duration of annealing, after annealing the sample to 920 K, the island area fraction decreases to 0.29. Higher triangular shaped areas emerge within the NbS_2 islands [Figure 2b]. In these areas, height profiles give an increased apparent height of $d' = 0.99$ nm at $V_s = 1.00 \text{ V}$ ($d' = 0.90$ nm at $V_s = -1.00 \text{ V}$). This height is inconsistent with bilayer NbS_2 , which has an apparent height of 1.22 nm at $V_s = 1.00 \text{ V}$, as displayed in Figure S1 in the SI. These higher areas are designated as in the $\sqrt{3} \times \sqrt{3}$ - phase, since below it will be shown

that they exhibit a $(\sqrt{3} \times \sqrt{3})\text{R}30^\circ$ superstructure and are of composition $\text{Nb}_{5/3}\text{S}_3\text{-2D}$.

After annealing the sample to 1020 K [Figure 2c], all islands display an apparent height of $d' = 0.99$ nm, consistent with the assumption that the islands have entirely transformed to the $\sqrt{3} \times \sqrt{3}$ - phase, indicating phase purity. The island area fraction decreased further to 0.17.

At first glance, annealing the sample to 1120 K as shown in Figure 2d does not change the situation. From the height profile, all islands still display a height $d' = 0.99$ nm characteristic of the $\sqrt{3} \times \sqrt{3}$ - phase. The islands shape is more regular, mostly hexagonal. However, the island area fraction further decreases to 0.12 and new features appear as highlighted by the white arrow. It marks a peninsula at-

tached to an Ir step edge. This and other peninsulas are attributed to Nb that penetrated the Gr sheet and attached to a step on Ir(111). Indeed, metal deposited or liberated from a TMDC layer on Gr/Ir(111) intercalates at elevated temperatures.^{24–26}

The $\sqrt{3} \times \sqrt{3}$ - phase islands are easy to shift laterally as a whole by the STM tip (see Figure S2a in the SI) consistent with being physisorbed to Gr. The liberated Gr, initially under an island, displays neither structural nor height changes. Thereby, it is ruled out that the height increase to $d' = 0.99$ nm is caused by changes in the Gr height level, *e.g.*, by intercalation of S or Nb underneath the islands.

After annealing to 1220 K [Figure 2e] the island area fraction is further reduced to 0.10. Two different height levels are present, neither of which coincides with the aforementioned ones. As obvious from the height profile, the dominant height level is $d' = 0.93$ nm at $V_s = 1.00$ V ($d' = 0.94$ nm at $V_s = -1.00$), slightly, but clearly, lower than the $\sqrt{3} \times \sqrt{3}$ - phase height. We designate areas with this height level as 1×1 - phase, since below it will be shown that they exhibit no superstructure and are of composition Nb_2S_3 -2D.

In addition to Nb intercalation peninsulas attached to Ir steps (white arrow) already observed after annealing to 1120 K, stripes and patches with an apparent height of about 0.1 nm with respect to the Gr base level are prominent now. In LEED this new intercalation feature gives rise to $(\sqrt{3} \times \sqrt{3})\text{R}30^\circ$ spots with respect to Ir(111) [compare Figure S3 in the SI]. Sulfur is well known to form a $(\sqrt{3} \times \sqrt{3})\text{R}30^\circ$ superstructure on Ir(111) and between Ir(111) and Gr.²⁷ Thus, these stripes and patches are due to S intercalation between Gr and Ir(111). A few of these intercalation stripes are already present at lower annealing temperature [compare Figure 2d]. Sulfur intercalation between Gr and Ir(111) is similarly observed after growth and annealing of other TMDCs.²⁶

The final annealing step to 1320 K leads to the complete decomposition of NbS_2 and no more Nb-S islands are visible, see Figure 2f. What remains is metallic Nb clusters as well as inter-

calated S and Nb.

To justify the designation of the 0.99 nm or 0.93 nm high islands as being $\sqrt{3} \times \sqrt{3}$ - phase or 1×1 - phase, we present atomically resolved STM images of the island structures from Figures 2a, c and e. For reference, Figure 3a displays atomically resolved NbS_2 . It has a lattice parameter of 0.331(3) nm as established in our previous work,¹⁹ in good agreement with values found for the single-layer NbS_2 on bilayer Gr/6H-SiC(0001) (0.334 nm)¹⁸ and bulk 2H- NbS_2 (0.3324 nm).¹⁶ The atomic corrugation is on the order of 35 pm as apparent from the height profile along the black line shown below the topograph. The height modulation on a length scale of ≈ 2.5 nm is due to the Gr/Ir(111) moiré pattern imposed on NbS_2 .^{19,26}

An atomically resolved topograph of the $\sqrt{3} \times \sqrt{3}$ - phase is shown in Figure 3b. It displays a clear $(\sqrt{3} \times \sqrt{3})\text{R}30^\circ$ superstructure with respect to the original NbS_2 lattice. Since all atoms in the top layer can still be recognized, the superstructure results from a trimerization of the S atoms. At the island edges the trimerization seems to fade away. The superstructure is associated with a height modulation on the order of 15 pm. The superstructure displays a lattice size of 0.577 ± 0.05 nm, which corresponds to $\sqrt{3}a$, with $a = 0.333 \pm 0.03$ nm. LEED obtained after annealing to 1020 K displays faint spots of a $(\sqrt{3} \times \sqrt{3})\text{R}30^\circ$ superstructure with respect to NbS_2 [Figure S3 in the SI].

Figure 3c shows an atomically resolved topograph of the 1×1 - phase. It features a 1×1 structure with the lattice parameter $a = 0.330 \pm 0.05$ nm, identical to the one of single-layer NbS_2 within the limits of error. The 1×1 - phase is distinct from pristine NbS_2 because: (i) it differs in height (0.93 nm vs. 0.62 nm); (ii) the atomic corrugation is only in the order of 5 pm, reduced by about a factor of 7 compared to the pristine NbS_2 ; and (iii) the Gr/Ir(111) moiré corrugation is shining through the 1×1 - phase islands is considerably damped compared to NbS_2 .

In order to obtain complementary chemical information about the annealing-induced phases, X-ray photoemission spectroscopy (XPS) of the S 2p, Nb 3d, C 1s, and Ir 4f

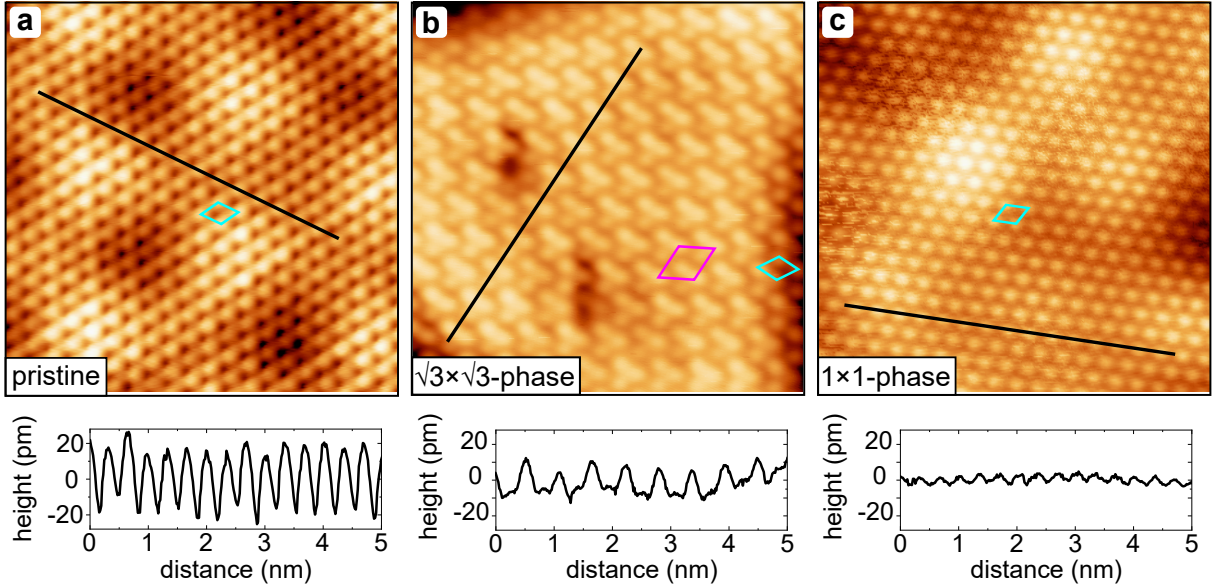


Figure 3: Atomic resolution STM topographs of (a) pristine single-layer NbS_2 , (b) the $\sqrt{3} \times \sqrt{3}$ - phase, and (c) the 1×1 - phase taken at 1.7 K. In the STM topographs the unit cells of the three phases are indicated by cyan rhomboids. Magenta rhomboid is the $(\sqrt{3} \times \sqrt{3})R30^\circ$ superstructure. Height profiles along the black lines are shown below the topographs. Image information: for all size $6 \text{ nm} \times 6 \text{ nm}$ and $T_s = 1.7 \text{ K}$, (a) $V_s = 50 \text{ mV}$, $I_t = 0.5 \text{ nA}$; (b) $V_s = 100 \text{ mV}$, $I_t = 0.80 \text{ nA}$; (c) $V_s = 100 \text{ mV}$, $I_t = 0.70 \text{ nA}$.

core levels was performed. Figure 4a shows the S 2p core-level spectra of samples with increasing annealing temperatures from 720 K (top) to 1370 K (bottom). The S 2p core level is spin-orbit split into a $2p_{3/2}$ and $2p_{1/2}$ doublet with an energy separation of $1.19(3) \text{ eV}$. The S 2p components are referenced in the following to the lower binding energy $2p_{3/2}$ peak. The appearance of the spectra has three distinct temperature ranges: (i) 720 K up to 870 K (yellow bar), (ii) 970 K to 1070 K (green bar), and (iii) 1170 K to 1220 K (orange bar). These temperature ranges agree well with the temperature ranges of the phases identified in STM (compare Figure 2). The distinct spectra for each temperature range is evidence of phase purity. The sequence of spectra shows a decrease in S 2p intensity with temperature (see also Figure S4 in the SI), and after annealing at 1320 K the S 2p signal has nearly vanished consistent with the decomposition of Nb-S compounds and subsequent S desorption. Spectra for Nb 3d, C 1s, and Ir 4f core-levels are displayed in Figure S5 of the SI.

The spectra in Figure 4b,c,d correspond to

single-layer NbS_2 , $\sqrt{3} \times \sqrt{3}$ - phase, and 1×1 - phase, respectively. The S 2p spectrum of NbS_2 in Figure 4b displays mainly a single spin-orbit doublet (yellow), designated S_{NbS_2} and located at $160.60(0) \text{ eV}$. The S_{NbS_2} component is attributed to top and bottom S in NbS_2 . In the $\sqrt{3} \times \sqrt{3}$ - phase spectrum after annealing to 1020 K in Figure 4c the S_{NbS_2} component is absent and two new main components are present: $S_{\text{top}-\sqrt{3}}$ at 161.33 eV (green) and S_{btw} at 163.08 eV (olive).

The substantial core level shifts are consistent with a phase transformation from NbS_2 to the $\sqrt{3} \times \sqrt{3}$ - phase. Having the largest intensity, the $S_{\text{top}-\sqrt{3}}$ component is associated with the top sulfur layer. The S_{btw} component (olive) with a significant core level shift of 2.48 eV compared to S_{NbS_2} is tentatively assigned to sulfur in a lower atomic plane (due to its lower intensity) and in a very different chemical environment than in NbS_2 . The origin of the S_{btw} will be clarified further below with the help of additional information from STM and DFT. The gray S_{int} component at 161.99 eV is attributed to intercalated S lost during the phase transfor-

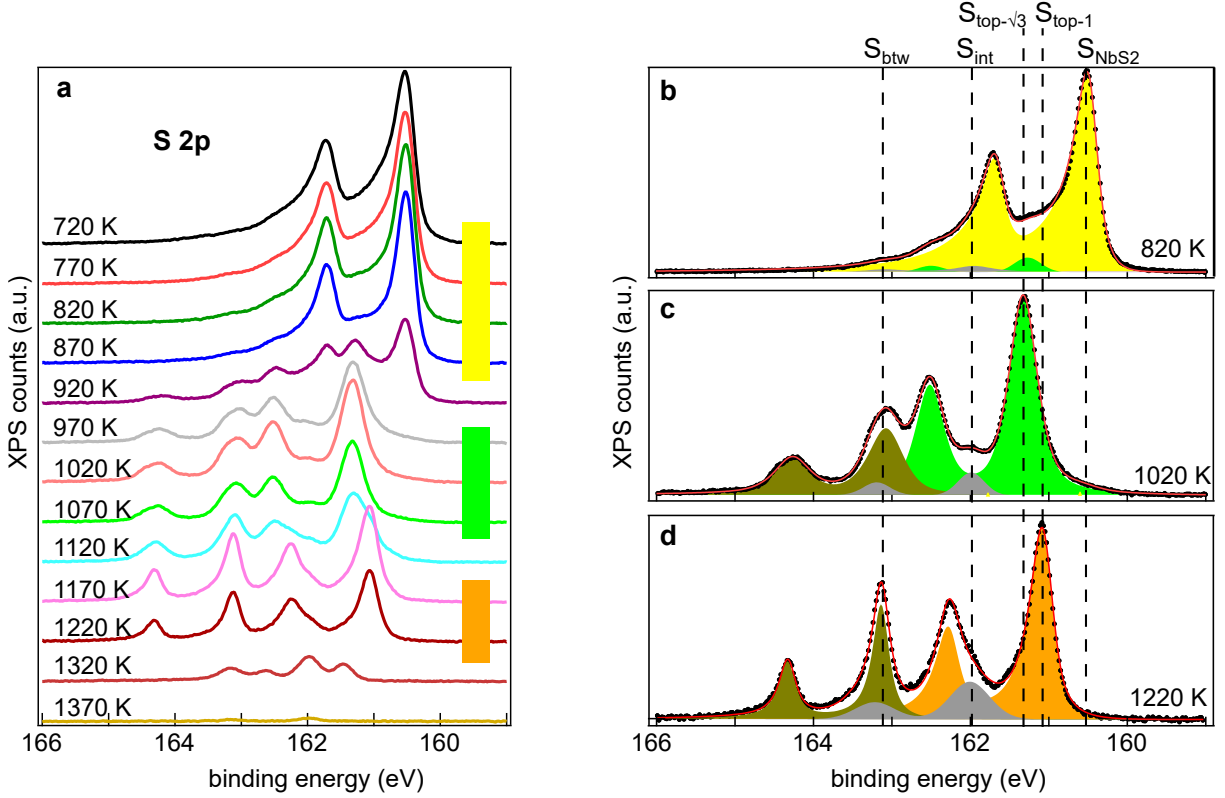


Figure 4: (a) XPS of the S 2p core level of initial single-layer NbS₂ on Gr/Ir(111) transformed during annealing. After room temperature growth, for each spectrum the sample was annealed to the indicated temperature without supply of additional S and cooled down to 300 K for measurements. The spectra are grouped in three temperature ranges according to their similarities: yellow, green, and orange. (b)-(d) S 2p core level spectra after annealing to (b) 820 K, (c) 1020 K, and (d) 1220 K fitted with components.

mation. The same S 2p component growing in intensity during annealing has been found for VS₂.¹¹

The 1×1 - phase spectrum after annealing to 1220 K in Figure 4d retains the S_{btw} component at 163.13 eV (olive) and develops a new $S_{\text{top-1}}$ component at 161.05 eV (orange), shifted by 0.28 eV with respect to the $S_{\text{top-}\sqrt{3}}$ component. Overall, the spectrum is quite similar to the $\sqrt{3} \times \sqrt{3}$ - phase spectrum and distinct from the NbS₂-spectrum. Remarkably, the $S_{\text{top-1}}$ and S_{btw} components are sharp with full width at half maximum (FWHM) of 0.29 eV and 0.27 eV, almost halved compared to the $\sqrt{3} \times \sqrt{3}$ - phase. The narrow peaks indicate the homogeneous state of the S in this phase. The S_{int} component is further increased due to the release of sulfur during the transformation from the $\sqrt{3} \times \sqrt{3}$ - phase to the 1×1 - phase.

Covalent transformation of NbS₂ by Nb vapor supply

The phase transformations of NbS₂ are likely to be triggered by Nb excess resulting from the loss of S due to annealing. If this rationale is correct, one could expect the transformation also to take place already at temperatures below T_{diss} , if additional Nb is supplied. Moreover, by controlling the amount of Nb supplied, it might be possible to select the resulting phase.

To test this idea, 0.12 ML Nb was deposited at 820 K on pre-grown single-layer NbS₂ islands with an area fraction of 0.36 [Figure 5a]. Plain annealing at 820 K neither causes NbS₂ dissociation nor changes the coverage fraction. Upon deposition of Nb, the single-layer NbS₂ transforms into the $\sqrt{3} \times \sqrt{3}$ - phase [Figure 5b]: the island height increased to 0.99 nm and the atomic resolution inset displays a ($\sqrt{3} \times$

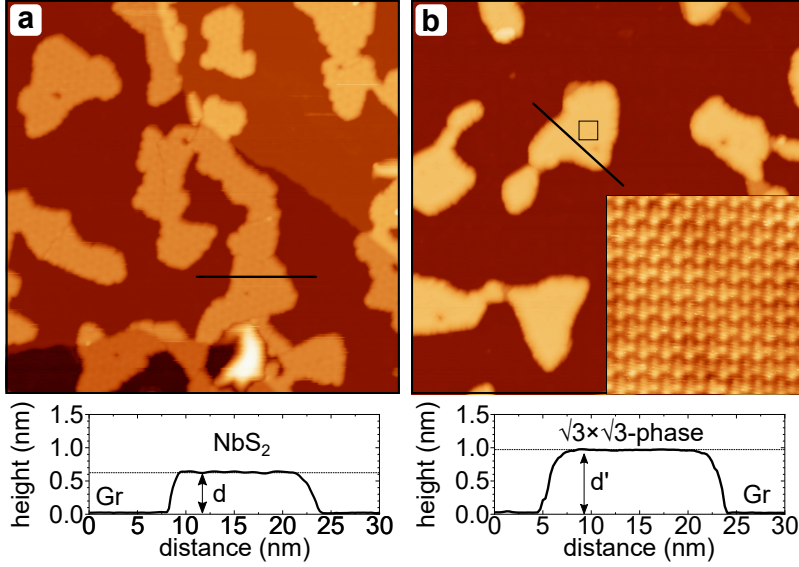


Figure 5: Formation of the $\sqrt{3} \times \sqrt{3}$ - phase by Nb supply. (a) Single-layer NbS₂ grown by deposition of 0.36 ML Nb in S background pressure at room temperature and annealed to 820 K in the absence of additional S supply. (b) Sample after deposition of additional 0.12 ML Nb at 820 K in the absence of additional S supply. Inset: atomic resolution topograph of boxed area. Height profiles are taken along the black lines in the STM topographs. Image information: (a) size 100 nm \times 100 nm, $V_s = 1.0$ V, $I_t = 1.00$ nA; (b) size 100 nm \times 100 nm, $V_s = 1.0$ V, $I_t = 1.0$ nA; Inset: 5 nm \times 5 nm, $V_s = 0.1$ V, $I_t = 5$ nA.

$\sqrt{3}$)R30° superstructure. The island area fraction decreased from 0.36 to 0.28. This titration experiment allows one to calculate the amount of Nb per unit cell in the $\sqrt{3} \times \sqrt{3}$ - phase. The total amount of Nb provided consists of 0.36 ML + 0.12 ML while the island area fraction is 0.28. Thus, each $\sqrt{3} \times \sqrt{3}$ - phase unit cell contains $x = \frac{0.36+0.12}{0.28}$ or $x = 1.71$ Nb atoms within the limits of error. It appears likely that $x = 5/3$ due to a full Nb layer and an additional $2/3$ Nb layer. Provided the $1/3$ vacancies order, they could give rise to the $\sqrt{3} \times \sqrt{3}$ superstructure of the $\sqrt{3} \times \sqrt{3}$ - phase.

Similarly, we deposited 0.33 ML Nb at 820 K on pre-grown pristine single-layer NbS₂ islands with an area fraction of 0.33 [Figure 6a]. As apparent from Figure 6b, upon deposition the NbS₂ islands transformed to the 1×1 - phase: the island height increased to 0.93 nm and the atomic resolution inset displays a 1×1 structure with low corrugation. Additionally, small clusters of large height are present at the island edges. The island area fraction marginally decreased from 0.33 to 0.29. With the same approach as above, one obtains formally an Nb

content of 2.3 atoms per 1×1 - phase unit cell. We tentatively conclude that a 1×1 - phase unit cell contains 2 Nb atoms while the excess Nb is contained in the metallic clusters. The sample remains in the 1×1 - phase upon additional annealing to 1020 K while the clusters at the island edges largely disappear [compare Figure 6c]. Their disappearance is presumably due to Nb already escaping under Gr at 1020 K.

It is remarkable that the 1×1 - phase forms at 820 K when excess Nb is supplied, whereas plain annealing requires 1220 K. The kinetically difficult process in phase formation during annealing under sulfur-poor conditions appears to be the release of Nb rather than reorganization of the initial NbS₂ islands.

XPS corroborates the transformation of NbS₂ to the 1×1 - phase using the same conditions as for the STM sequence presented in Figure 6. Figure 7a shows the typical S 2p spectrum for pristine NbS₂, similar to Figure 4b. After deposition of Nb at 820 K, the spectrum in Figure 7b is nearly identical to the spectrum obtained after annealing to 1220 K in the absence of Nb supply [compare Fig-

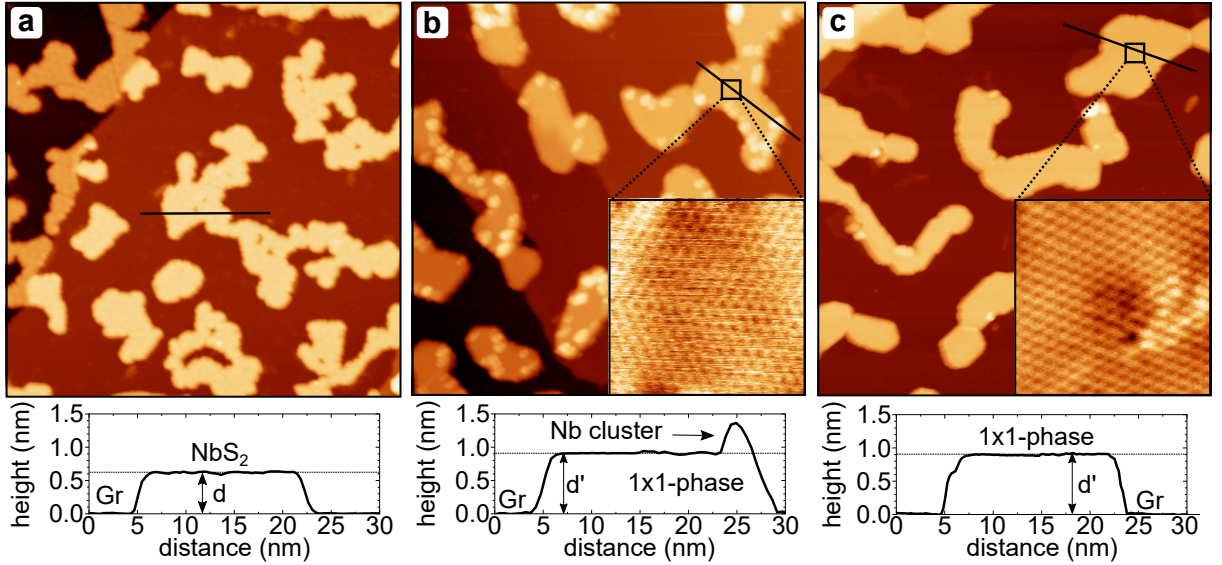


Figure 6: Formation of the 1×1 - phase by Nb supply. (a) Single-layer NbS_2 grown by deposition of 0.33 ML Nb in S background pressure at room temperature and annealed to 820 K in the absence of additional S supply. (b) Sample after deposition of additional 0.33 ML Nb at 820 K. Inset: atomic resolution topograph of the boxed area. (c) Sample after additional annealing to 1020 K. Inset: atomic resolution STM topograph of the boxed area. Height profiles are taken along the black lines in the topographs. Image information: (a) size $100 \text{ nm} \times 100 \text{ nm}$, $V_s = 1.0 \text{ V}$, $I_t = 0.23 \text{ nA}$; (b) size $100 \text{ nm} \times 100 \text{ nm}$, $V_s = 1.0 \text{ V}$, $I_t = 0.3 \text{ nA}$; Inset: $5 \text{ nm} \times 5 \text{ nm}$, $V_s = 0.1 \text{ V}$, $I_t = 5 \text{ nA}$; (c) size $100 \text{ nm} \times 100 \text{ nm}$, $V_s = 1.2 \text{ V}$, $I_t = 0.3 \text{ nA}$; Inset: $5 \text{ nm} \times 5 \text{ nm}$, $V_s = 0.1 \text{ V}$, $I_t = 5 \text{ nA}$.

ure 4d] being characteristic of the 1×1 - phase. Upon further annealing to 1020 K, the 1×1 - phase remains unchanged and the related spectrum in Figure 7c is indistinguishable from the one obtained after 1×1 - phase formation at 1220 K without additional Nb supply shown in Figure 4d.

DFT calculations

With the experimental information at hand and the help of density functional theory (DFT) calculations we determined the structure of the 2D materials resulting from phase transformations of NbS_2 . We start the analysis with the 1×1 - phase.

The 1×1 - phase has the following properties: (i) hexagonal symmetry and lattice parameter identical to single-layer NbS_2 within the limits of error; (ii) it contains a smaller fraction of sulfur than NbS_2 and even less than the $\sqrt{3} \times \sqrt{3}$ - phase, since it evolves upon annealing from these phases under sulfur-deficient conditions, accompanied by a gradual decrease of the S 2p

intensity; (iii) apparent height 0.93 nm, larger by 0.31 nm compared to NbS_2 ; (iv) 2 Nb atoms per unit cell; (v) no superstructure; (vi) only physisorbed to Gr.

It is well known from the Nb-S phase diagram and previous reports^{21,22} that at high temperatures in bulk a NiAs-type structure of NbS forms, with almost identical lattice parameter as NbS_2 . The NiAs structure is hexagonal, with As atoms forming a hexagonal close-packed lattice, with Ni in octahedral sites, resulting in alternating atomic planes of Ni and As. Since the 1×1 - phase contains two Nb atoms per unit cell, a natural starting point for the DFT calculations was just the NbS bulk unit cell, *i.e.*, Nb_2S_2 -2D.

The minimum energy configuration of Nb_2S_2 -2D on Gr is surprisingly not of NiAs-type. It consists of two Nb layers in trigonal prismatic coordination with the S atoms as well as the Nb atoms of the respective layers sitting atop each other, as shown in the ball model insets of Figure 8. For higher energy structures compare Table S1 in the SI. The ground state con-

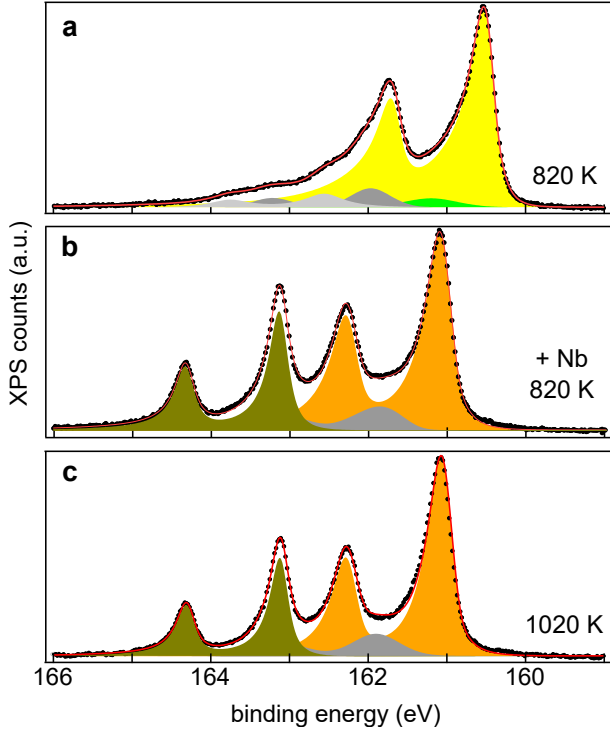


Figure 7: (a) High-resolution XPS of the S 2p core level of NbS₂ on Gr/Ir(111). (b) After deposition of additional Nb at 820 K. (c) After annealing at 1020 K. Fit of each spectrum with five S 2p components.

figuration (i.e., the lowest energy structure) is chemisorbed to Gr with Nb-plane to Gr distance of only 0.22 nm. However, our calculations also identified a local minimum configuration in which the Nb₂S₂-2D layer is physisorbed at a distance of 0.36 nm. Furthermore, starting from the chemisorbed configuration and rigidly lifting the Nb₂S₂-2D above the Gr we evaluated the total energy of the system at specific distances along the z -direction. Figure 8 shows the total slab energy versus distance. No significant barrier exists between the physisorbed and the chemisorbed state. As an additional note, the chemisorption of hypothetical Nb₂S₂-2D to Gr is not surprising, given the expected high reactivity of the bare Nb (i.e., a 4d metal) towards the C atoms of Gr. Considering the high temperatures used in our experiments, one expects that any potential barrier between physisorbed and chemisorbed state can be overcome. Therefore Nb₂S₂-2D should be chemisorbed to Gr. Given that the 1×1 -phase islands are easy to move with the STM

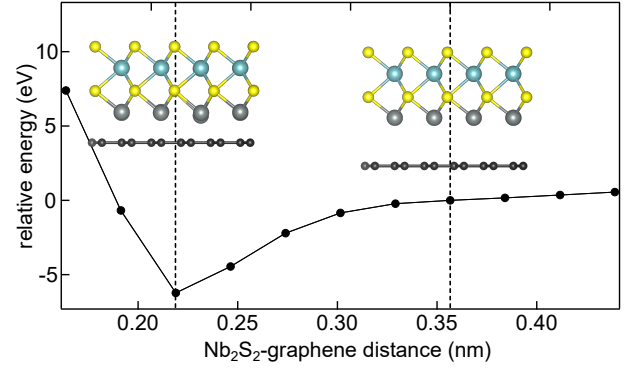


Figure 8: Chemisorption of Nb₂S₂-2D to Gr. Relative total energy of minimum energy configuration of Nb₂S₂-2D (lowest energy structure) as a function of the distance to Gr. Zero point of the energy scale is at 0.36 nm in the physisorbed state. Inset: side view ball models of relaxed DFT geometries for Nb₂S₂-2D in the 0.36 nm and 0.22 nm Nb-C distances. Nb atoms: cadet blue balls and gray; S atoms: yellow; dark gray: C atoms.

tip on Gr [see Figure S2b in the SI] and that the C 1s core level is not affected during the phase transformations of physisorbed NbS₂ [compare Figure S4b in the SI], the 1×1 -phase is not chemisorbed. Thus, we can clearly exclude that the Nb₂S₂-2D is observed in our experiments, regardless of the stacking sequence.

As chemisorption has to be ruled out, we are forced to assume the presence of an additional passivating S layer, i.e., the 1×1 -phase to be Nb₂S₃-2D. Using DFT, all possible eight stacking sequences for Nb₂S₃-2D were calculated (compare Table S2 of the SI). Irrespective of the stacking, Nb₂S₃-2D is solely physisorbed to Gr, consistent with complete Nb passivation by S. The lowest energy structure is presented in Figure 9a and b as top and side view ball model. It is again not the expected NiAs-type structure, but displays all Nb atoms in trigonal prismatic coordination with the S and Nb atoms of the respective layers sitting atop each other. The structure possesses no reconstruction, as required. It has a lattice parameter of $a = 0.333$ nm in decent agreement with the experimental value of 0.330 nm. The calculated height of 0.976 nm matches reasonably well with the STM measured apparent heights of 0.93 nm

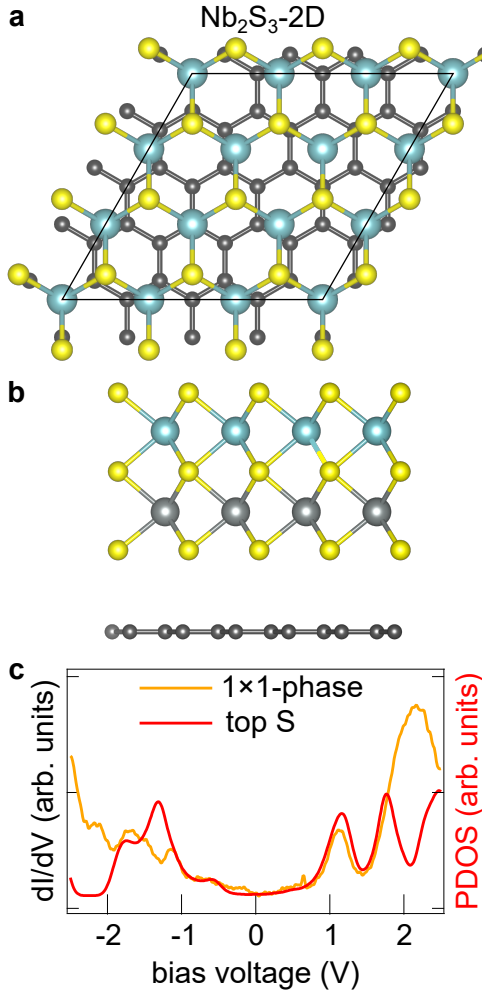


Figure 9: DFT calculated ball model representation of the 1×1 - phase with stoichiometry $\text{Nb}_2\text{S}_3\text{-2D}$ in (a) top and (b) side view. Nb atoms: cadet blue balls and gray; S atoms: yellow; dark gray: C atoms. (c) Differential conductance spectrum of the 1×1 - phase (orange) compared to the DFT calculated partial density of states (PDOS) of the topmost S atoms (red). Spectrum parameters are $V_{\text{stab}} = 2.5 \text{ V}$, $I_{\text{stab}} = 0.7 \text{ nA}$, $V_{\text{mod}} = 10 \text{ mV}$, $f_{\text{mod}} = 811 \text{ Hz}$, $T_s = 1.7 \text{ K}$.

at $+1.00 \text{ V}$ and 0.94 nm at -1.00 V . Figure 9c shows tmgood agreement between the calculated top-layer S partial density of states with a large-range differential conductance STS spectrum.

The interpretation of the S 2p core level components is now straightforward given the $\text{Nb}_2\text{S}_3\text{-2D}$ stoichiometry: The S_{btw} component at 163.13 eV strongly shifted by 2.48 eV with respect to S_{NbS_2} arises from S atoms lo-

cated between two Nb planes, which provides a more electropositive environment compared to S atoms with Nb neighbors on only one side. This explains the significant binding energy shift, indicating a substantially altered chemical environment. The $S_{\text{top-1}}$ component at 161.05 eV shifted by 0.45 eV with respect to S_{NbS_2} corresponds to the S top plane of atoms, while the bottom S atoms, with two Nb and two S atomic planes above, do not contribute significantly to the intensity due to substantial damping. The bottom S intensity is presumably hidden in the $S_{\text{top-1}}$ component.

The $\sqrt{3} \times \sqrt{3}$ - phase is quite similar to the 1×1 - phase in terms of symmetry, lattice parameter, apparent height (0.99 nm), and the overall shape of the S 2p core-level spectra. However, it displays a $\sqrt{3} \times \sqrt{3}$ superstructure and contains only about $5/3$ Nb atoms per unit cell. From previous work²¹ it is known that in the NiAs-type bulk structures of stoichiometry $\text{Nb}_{2-x}\text{S}_2$, Nb vacancies are present in every second Nb layer.

For the $\sqrt{3} \times \sqrt{3}$ - phase it is therefore most reasonable to assume that $1/3$ of Nb is missing in one of the two Nb layers. This pattern would naturally give rise to the $\sqrt{3} \times \sqrt{3}$ superstructure, which is observed in LEED and STM. The stoichiometry of the $\sqrt{3} \times \sqrt{3}$ - phase is consequently $\text{Nb}_{5/3}\text{S}_3\text{-2D}$.

The lowest energy structure of $\text{Nb}_{5/3}\text{S}_3\text{-2D}$ is displayed in Figure 10a and b as top and side view ball model (compare Table S3 of the SI for other calculated structures). Again, the minimum energy is not a NiAs-type structure. While the Nb atoms in the complete atomic plane close to Gr are still in trigonal prismatic coordination, the top Nb plane with the regularly distributed Nb vacancies has the Nb atoms in octahedral coordination. The structure displays a $\sqrt{3} \times \sqrt{3}$ superstructure, as required. It has a lattice parameter of 0.333 nm , in agreement with the experimental value of 0.333 nm . The calculated height of 0.964 nm matches reasonably well with the average of the STM measured apparent heights of 0.99 nm at $+1.00 \text{ V}$ and 0.90 nm at -1.00 V . Figure 10c shows decent agreement of the calculated top S partial density of states with a large-range differential con-

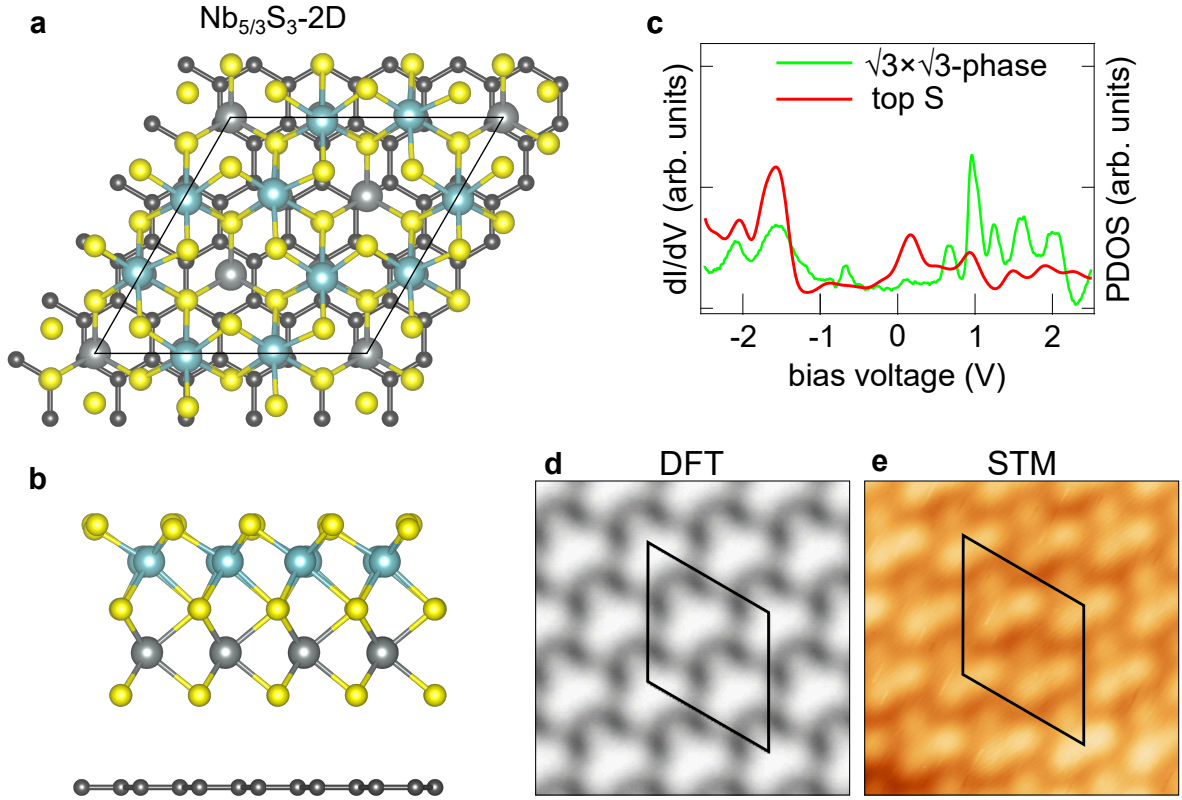


Figure 10: DFT calculated ball model representation of the $\sqrt{3} \times \sqrt{3}$ - phase with stoichiometry $\text{Nb}_{5/3}\text{S}_3\text{-2D}$ in (a) top and (b) side view. Nb atoms: cadet blue balls and gray; S atoms: yellow; dark gray: C atoms. (c) Differential conductance spectrum of the $\sqrt{3} \times \sqrt{3}$ - phase (green) compared to the DFT calculated partial density of states (PDOS) of the topmost S atoms (red). (d) DFT calculated STM topograph compared to (e) measurement. Spectrum parameters: $V_{\text{stab}} = 3 \text{ V}$, $I_{\text{stab}} = 0.8 \text{ nA}$, $V_{\text{mod}} = 10 \text{ mV}$, $f_{\text{mod}} = 797 \text{ Hz}$, $T_s = 1.7 \text{ K}$.

ductance STS spectrum, reproducing the number of peaks on the unoccupied region, but not their location nor intensity. Figure 10d and e show excellent agreement between the DFT simulated STM topograph and the measurement.

The S 2p spectrum of the $\sqrt{3} \times \sqrt{3}$ - phase is interpreted as follows: the $S_{\text{top}-\sqrt{3}}$ component at 161.33 eV is assigned to top sulfur, while the S_{btw} component corresponds to the highly coordinated sulfur atoms between Nb atomic planes. The larger FWHM of both components for the $\sqrt{3} \times \sqrt{3}$ - phase, compared to the 1×1 - phase, indicates a less homogeneous state of sulfur, which due to the Nb vacancies, are bound to fewer Nb atoms on one side.

Summary

Under sulfur-poor conditions and heating single-layer NbS_2 transforms to the more Nb-rich compounds $\text{Nb}_{5/3}\text{S}_3\text{-2D}$ (1020 K, $\sqrt{3} \times \sqrt{3}$ - phase) and $\text{Nb}_2\text{S}_3\text{-2D}$ (1220 K, 1×1 - phase). $\text{Nb}_{5/3}\text{S}_3\text{-2D}$ displays a $\sqrt{3} \times \sqrt{3}$ superstructure caused by regularly arranged Nb vacancies in the top Nb layer. The same compounds may also be created by deposition of excess Nb under sulfur-poor conditions at 820 K, a temperature at which NbS_2 does not show changes with time in the absence of a Nb flux. The compounds consist of two Nb layers sandwiched between three S layers and are inert, covalently bound 2D materials. Consequently, these compounds emerge from NbS_2 through covalent transformation. As uncovered by density functional theory calculations, the layer stacking sequence is unique for each compound and can not be de-

rived from corresponding bulk materials. Their ease of preparation and unexpected structures provide a new handle to tailor properties and create new functions of 2D layers.

Methods

The experiments were carried out in three ultrahigh vacuum systems (base pressure in low 10^{-10} mbar range). All systems were equipped with sample preparation and growth facilities as well as LEED. STM measurements were conducted in two systems in Cologne while XPS was performed at the FlexPES beamline end station at MAX IV Laboratory, Lund.

Ir(111) was cleaned by cycles of keV Ar^+ or Xe^+ sputtering and flash annealing to 1520 K. Gr was grown by ethylene exposure of Ir(111) to saturation at room temperature, subsequent flash annealing to 1470 K, and followed by exposure to ≈ 800 L of ethylene at 1370 K. As confirmed by STM and LEED a closed single crystal Gr monolayer on Ir(111) results.²⁸

Single-layer H-NbS₂ was prepared by exposing Gr/Ir(111) to a flux of $\approx 6 \times 10^{15}$ atoms/m²s Nb from an e-beam evaporator in a background pressure of $\approx 8 \times 10^{-9}$ mbar elemental S. The S was supplied by a pyrite filled Knudsen cell about 10 cm away from the sample. Growth was conducted for 510 s at room temperature, followed by 360 s annealing at 820 K. During annealing, the Knudsen cell was turned off. However, since the S pressure decreases slowly, the S pressure remained non-zero, albeit well below 8×10^{-9} mbar. Since H-NbS₂ growth takes place with excess S reevaporating, the amount of H-NbS₂ formed is characterized through the amount of Nb deposited. 1 monolayer (ML) of Nb corresponds to the Nb amount in a full single layer of NbS₂, *i.e.*, to 1.12×10^{19} atoms/m². Phase transformations of H-NbS₂ resulted from deposition of elemental Nb onto single-layer NbS₂ at different temperatures, or by annealing to temperatures above 820 K, or both, as specified where the respective data is discussed.

The samples were investigated *in situ* by STM, either at 300 K or at 1.7 K after ultrahigh vacuum transfer into a bath cryo-

stat. STS was conducted at 1.7 K with Au-covered W tips calibrated using the surface state of Au(111).^{29,30} Constant-current STM topographs were recorded with sample bias V_s and tunneling current I_t specified in each figure. dI/dV spectra were recorded with stabilization bias V_{stab} and stabilization current I_{stab} using a lock-in amplifier with a modulation frequency f_{mod} and modulation voltage V_{mod} , also specified in the captions.

The XPS experiments were conducted at the FlexPES beamline at MAX IV Laboratory, Lund, Sweden.³¹ The growth of Nb_xS_y-2D compounds at the beamline was carried out with a Nb evaporator calibrated by STM in the home lab. High-resolution XPS of core-levels was performed in normal emission geometry with a spot size of $50 \mu\text{m} \times 50 \mu\text{m}$ and at room temperature. The core levels were monitored with photon energies to maximize surface sensitivity: 150 eV for Ir 4f, 260 eV for S 2p, 380 eV for C 1s, 300 eV for Nb 3d. Overview spectra and high resolution O 1s spectra obtained at the first and last measurements of an annealing series confirmed that no other species were present. Curve fitting was performed with a pseudo-Voigt function. The asymmetry is included by an energy-dependent variation of the full-width-at-half maximum. The width, asymmetry and ratio of Gaussian to Lorentzian contributions were fixed for each component, meaning that they were not allowed to vary between spectra taken at different annealing temperatures. The center energy of each component was granted a ± 100 meV variation between different spectra while the intensities of the components were unconstrained.

Our spin-polarized calculations were done by using DFT³² and the projector augmented plane wave method³³ as implemented in the VASP code.^{34,35} We used a 500 eV energy cutoff for the plane wave expansion of the Kohn-Sham wave functions.³⁶ To account for the non-local correlation effects like van der Waals interactions,³⁷ all structural relaxations were done by using vdW-DF2³⁸ functional containing a revised Becke (B86b) exchange,^{39,40} while the analysis of the electronic structure was performed by using the standard PBE exchange-

correlation energy functional.⁴¹

Acknowledgement We acknowledge funding from Deutsche Forschungsgemeinschaft (DFG) through CRC 1238 (project number 277146847, subprojects A01, B06 and C01). W.J. acknowledges financial support from the DFG SPP 2244 (projects No. 535290457). J.K. acknowledges financial support from the Swedish Research Council, grant number 2022-04363. J.F. acknowledges financial support from the DFG through project FI 2624/1-1 (project No. 462692705) within the SPP 2137. MAX IV Laboratory is acknowledged for time on Beamline FlexPES under Proposal 20210859. Research conducted at MAX IV, a Swedish national user facility, is supported by the Swedish Research council under contract 2018-07152, the Swedish Governmental Agency for Innovation Systems under contract 2018-04969, and Formas under contract 2019-02496. The authors acknowledge computing time granted by the JARA Vergabegremium and provided on the JARA Partition part of the supercomputer JURECA at Forschungszentrum Jülich.

Supporting Information Available

Measurement of bilayer NbS₂, Nb_xS_y islands displaced by the STM tip, LEED of the $\sqrt{3} \times \sqrt{3}$ - phase, S 2p components as a function of temperature, Nb 3d, C 1s, and Ir 4f core-levels spectra as a function of temperature, DFT calculations of different Nb₂S₂-2D, Nb₂S₃-2D, and Nb_{5/3}S₃-2D structures on Gr.

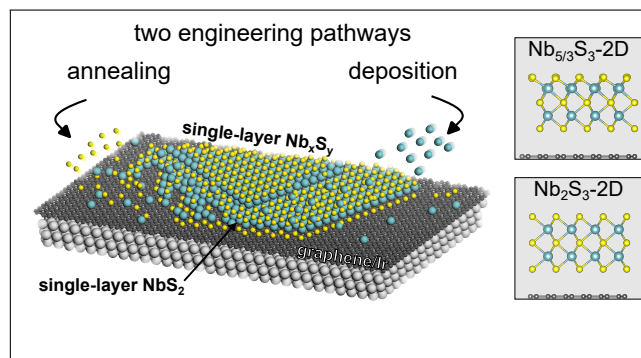
References

- (1) Huang, Y.; Sutter, E.; Shi, N. N.; Zheng, J.; Yang, T.; Englund, D.; Gao, H.-J.; Sutter, P. Reliable exfoliation of large-area high-quality flakes of graphene and other two-dimensional materials. *ACS Nano* **2015**, *9*, 10612–10620.
- (2) Huang, Y. et al. Universal mechanical exfoliation of large-area 2D crystals. *Nat. Commun.* **2020**, *11*, 2453.
- (3) Geim, A. K.; Grigorieva, I. V. Van der Waals heterostructures. *Nature* **2013**, *499*, 419–425.
- (4) Novoselov, K. S.; Mishchenko, A.; Carvalho, A.; Neto, A. H. C. 2D materials and van der Waals heterostructures. *Science* **2016**, *353*, aac9439.
- (5) Cao, Y.; Fatemi, V.; Demir, A.; Fang, S.; Tomarken, S. L.; Luo, J. Y.; Sanchez-Yamagishi, J. D.; Watanabe, K.; Taniguchi, T.; Kaxiras, E.; Ashoori, R. C.; Jarillo-Herrero, P. Correlated insulator behaviour at half-filling in magic-angle graphene superlattices. *Nature* **2018**, *556*, 80–84.
- (6) Wan, W.; Wickramaratne, D.; Dreher, P.; Harsh, R.; Mazin, I. I.; Ugeda, M. M. Nontrivial Doping Evolution of Electronic Properties in Ising-Superconducting Alloys. *Adv. Mater.* **2022**, *34*, 2200492.
- (7) Fortin-Deschênes, M.; Watanabe, K.; Taniguchi, T.; Xia, F. Van der Waals epitaxy of tunable moirés enabled by alloying. *Nat. Mater.* **2024**, *23*, 339–346.
- (8) Zhao, X. et al. Engineering covalently bonded 2D layered materials by self-intercalation. *Nature* **2020**, *581*, 171–177.
- (9) Liu, M.; Huang, Y. L.; Gou, J.; Liang, Q.; Chua, R.; Arramel; Duan, S.; Zhang, L.; Cai, L.; Yu, X.; Zhong, D.; Zhang, W.; Wee, A. T. S. Diverse Structures and Magnetic Properties in Nonlayered Monolayer Chromium Selenide. *J. Phys. Chem. Lett.* **2021**, *12*, 7752–7760.
- (10) Arnold, F. et al. Novel single-layer vanadium sulphide phases. *2D Mater.* **2018**, *5*, 045009.
- (11) van Efferen, C.; Hall, J.; Atodiressei, N.; Boix, V.; Safeer, A.; Wekking, T.; Vinogradov, N. A.; Preobrajenski, A. B.; Knudsen, J.; Fischer, J.; Jolie, W.;

- Michely, T. 2D vanadium sulfides: synthesis, atomic Structure engineering, and charge density Waves. *ACS Nano* **2024**, *18*, 14161–14175.
- (12) Lasek, K.; Ghorbani-Asl, M.; Pathirage, V.; Krashennnikov, A. V.; Batzill, M. Controlling stoichiometry in ultrathin van der Waals Films: PtTe₂, Pt₂Te₃, Pt₃Te₄, and Pt₂Te₂. *ACS Nano* **2022**, *16*, 9908–9919.
 - (13) Zhang, Z.-M.; Gong, B.-C.; Nie, J.-H.; Meng, F.; Zhang, Q.; Gu, L.; Liu, K.; Lu, Z.-Y.; Fu, Y.-S.; Zhang, W. Self-intercalated 1T-FeSe₂ as an Effective Kagome Lattice. *Nano Lett.* **2023**, *23*, 954–961.
 - (14) Khatun, S.; Alanwoko, O.; Pathirage, V.; de Oliveira, C. C.; Tromer, R. M.; Autreto, P. A. S.; Galvao, D. S.; Batzill, M. Solid State Reaction Epitaxy, A New Approach for Synthesizing Van der Waals heterolayers: The case of Mn and Cr on Bi₂Se₃. *Adv. Funct. Mater.* **2024**, 2315112.
 - (15) Van Maaren, M. H.; Schaeffer, G. M. Superconductivity in group Va dichalcogenides. *Phys. Lett.* **1966**, *20*, 131.
 - (16) Fisher, W. G.; Sienko, M. J. Stoichiometry, structure, and physical properties of niobium disulfide. *Inorganic Chemistry* **1980**, *19*, 39–43.
 - (17) Witteveen, C.; Górnicka, K.; Chang, J.; Månsson, M.; Klimczuk, T.; von Rohr, F. O. Polytypism and superconductivity in the NbS₂ system. *Dalton Trans.* **2021**, *50*, 3216–3223.
 - (18) Lin, H.; Huang, W.; Zhao, K.; Lian, C.; Duan, W.; Chen, X.; Ji, S. H. Growth of atomically thick transition metal sulfide films on graphene/6H-SiC(0001) by molecular beam epitaxy. *Nano Res.* **2018**, *11*, 4722–4727.
 - (19) Knispel, T.; Berges, J.; Schobert, A.; van Loon, E. G. C. P.; Jolie, W.; Wehling, T.; Michely, T.; Fischer, J. Unconventional Charge-Density-Wave Gap in Monolayer NbS₂. *Nano Lett.* **2024**, *24*, 1045–1051.
 - (20) Yang, J.; Mohmad, A. R.; Wang, Y.; Fullon, R.; Song, X.; Zhao, F.; Bozkurt, I.; Augustin, M.; Santos, E. J.; Shin, H. S.; Zhang, W.; Voiry, D.; Jeong, H. Y.; Chhowalla, M. Ultrahigh-current-density niobium disulfide catalysts for hydrogen evolution. *Nat. Mater.* **2019**, *18*, 1309–1314.
 - (21) Jellinek, F.; Brauer, G.; Müller, H. Molybdenum and Niobium Sulphides. *Nature* **1960**, *185*, 376–377.
 - (22) Kadijk, F.; Jellinek, F. The system niobium-sulfur. *J. Less-common metals* **1969**, *19*, 421–430.
 - (23) Stan, R.-M.; Mahatha, S. K.; Bianchi, M.; Sanders, C. E.; Curcio, D.; Hofmann, P.; Miwa, J. A. Epitaxial single-layer NbS₂ on Au(111): Synthesis, structure, and electronic properties. *Phys. Rev. Mater.* **2019**, *3*, 44003.
 - (24) Schumacher, S.; Förster, D. F.; Rösner, M.; Wehling, T. O.; Michely, T. Strain in Epitaxial Graphene Visualized by Intercalation. *Phys. Rev. Lett.* **2013**, *110*, 086111.
 - (25) Martínez-Galera, A. J.; Schröder, U. A.; Herbig, C.; Arman, M. A.; Knudsen, J.; Michely, T. Preventing sintering of nanoclusters on graphene by radical adsorption. *Nanoscale* **2017**, *9*, 13618–13629.
 - (26) Hall, J.; Pielic, B.; Murray, C.; Jolie, W.; Wekking, T.; Busse, C.; Kralj, M.; Michely, T. Molecular beam epitaxy of quasi-freestanding transition metal disulfide monolayers on van der Waals substrates: a growth study. *2D Mater.* **2018**, *5*, 25005.
 - (27) Pielic, B.; Hall, J.; Despoja, V.; Rakić, I. Š.; Petrović, M.; Sohani, A.; Busse, C.; Michely, T.; Kralj, M. Sulfur Structures on Bare and Graphene-Covered

- Ir(111). *J. Phys. Chem. C* **2020**, *124*, 6659–6668.
- (28) van Gastel, R.; N’Diaye, A. T.; Wall, D.; Coraux, J.; Busse, C.; Buckanie, N. M.; zu Heringdorf, F.-J.; von Hoegen, M.; Michely, T.; Poelsema, B. Selecting a single orientation for millimeter sized graphene sheets. *Appl. Phys. Lett.* **2009**, *95*, 121901.
- (29) Kaiser, W. J.; Jaklevic, R. C. Spectroscopy of electronic states of metals with a scanning tunneling microscope. *IBM J. Res. Dev.* **1986**, *30*, 411–416.
- (30) Everson, M. P. Effects of surface features upon the Au(111) surface state local density of states studied with scanning tunneling spectroscopy. *J. Vac. Sci. Technol.* **1991**, *9*, 891.
- (31) Preobrajenski, A.; Generalov, A.; Öhrwall, G.; Tchapyguine, M.; Tarawneh, H.; Appelfeller, S.; Framp-ton, E.; Walsh, N. FlexPES: a versatile soft X-ray beamline at MAXIV Laboratory. *J. Synchrotron Rad.* **2023**, *30*, 831–840.
- (32) Hohenberg, P.; Kohn, W. Inhomogeneous electron gas. *Phys. Rev.* **1964**, *136*, B864.
- (33) Blöchl, P. E. Projector augmented-wave method. *Phys. Rev. B* **1994**, *50*, 17953.
- (34) Kresse, G.; Hafner, J. Ab initio molecular dynamics for liquid metals. *Phys. Rev. B* **1993**, *47*, 558.
- (35) Kresse, G.; Furthmüller, J. Ab initio molecular dynamics for liquid metals. *Phys. Rev. B* **1996**, *54*, 11169.
- (36) Kohn, W.; Sham, L. J. Self-consistent equations including exchange and correlation effects. *Phys. Rev.* **1965**, *140*, A1133.
- (37) Huttmann, F.; Martinez Galera, A. J.; Caciuc, V.; Atodiresei, N.; Schumacher, S.; Standop, S.; Hamada, I.; Wehling, T. O.; Blügel, S.; Michely, T. Tuning the van der Waals Interaction of Graphene with Molecules via Doping. *Phys. Rev. Lett.* **2015**, *115*, 236101.
- (38) Lee, K.; Murray, E. D.; Kong, L.; Lundqvist, B. I.; Langreth, D. C. Higher accuracy van der Waals density functional. *Phys. Rev. B* **2010**, *82*, 081101.
- (39) Becke, A. On the large-gradient behavior of the density functional exchange energy. *J. Chem. Phys.* **1986**, *85*, 7184.
- (40) Hamada, I. Higher-accuracy van der Waals density functional. *Phys. Rev. B* **2014**, *89*, 121103.
- (41) Perdew, J. P.; Burke, K.; Ernzerhof, M. Generalized gradient approximation made simple. *Phys. Rev. Lett.* **1996**, *77*, 3865.

TOC Graphic



Supplementary Information:

Engineering two-dimensional materials from single-layer NbS₂

Timo Knispel,[†] Daniela Mohrenstecher,[†] Carsten Speckmann,[†] Affan Safeer,[†]
Camiel van Efferen,[†] Virgínia Boix,[‡] Alexander Grüneis,[†] Wouter Jolie,[†] Alexei
Preobrajenski,[¶] Jan Knudsen,[‡] Nicolae Atodiresei,[§] Thomas Michely,[†] and
Jeison Fischer^{*,†}

[†]*II. Physikalisches Institut, Universität zu Köln, Zùlpicher Straße 77, D-50937 Cologne,
Germany*

[‡]*NanoLund and Division of Synchrotron Radiation Research, Department of Physics, Lund
University, SE-22100 Lund, Sweden*

[¶]*MAX IV Laboratory, Lund University, SE-221 00 Lund, Sweden*

[§]*Peter Grünberg Institut (PG-1), Forschungszentrum Jülich, Wilhelm-Johnen-Straße,
D-52428 Jülich, Germany*

E-mail: jfischer@ph2.uni-koeln.de

Contents

Supplementary Note 1: NbS ₂ bilayer islands after room temperature growth and annealing at 820 K	3
Supplementary Note 2: Nb _x S _y islands displaced by the STM tip	4
Supplementary Note 3: LEED of the $\sqrt{3} \times \sqrt{3}$ - phase	5
Supplementary Note 4: S 2p components and total S 2p core level intensity as a function of temperature during NbS ₂ transformation by annealing.	6
Supplementary Note 5: Nb 3d, C 1s, and Ir 4f core-levels as a function of temperature during NbS ₂ transformation by annealing.	7
Supplementary Note 6: DFT calculated Nb ₂ S ₂ -2D structures on Gr	8
Supplementary Note 7: DFT calculated Nb ₂ S ₃ -2D structures on Gr	9
Supplementary Note 8: DFT calculated Nb _{5/3} S ₃ -2D structures on Gr	10

Supplementary Note 1: NbS₂ bilayer islands after room temperature growth and annealing at 820 K

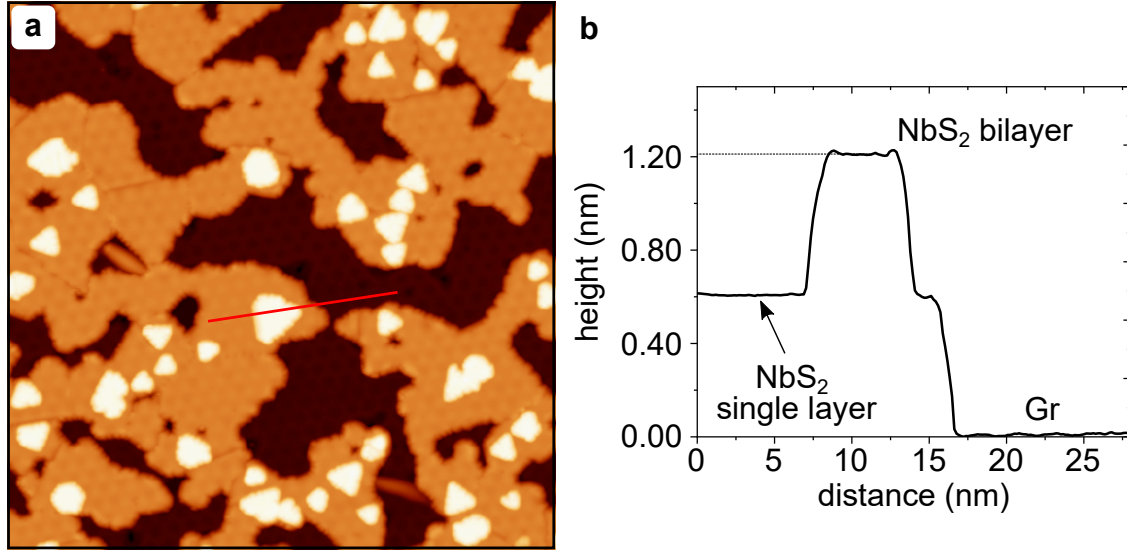


Figure S1: NbS₂ single layer and bilayer islands after growth on Gr/Ir(111) and annealing to 820 K. (a) STM topograph. (b) Height profile measured along the red line in (a). Image information: size 75 nm \times 75 nm, $V_s = 1.0$ V, $I_t = 0.1$ nA, $T_s = 0.4$ K

Supplementary Note 2: Nb_xS_y islands displaced by the STM tip

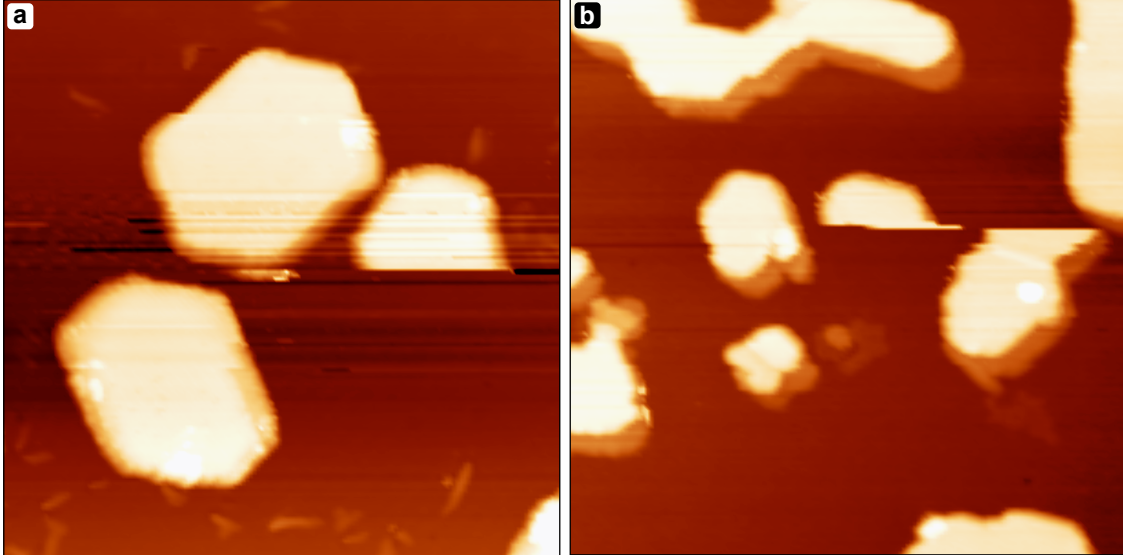


Figure S2: (a) Nb_2S_3 -2D and (b) $\text{Nb}_{5/3}\text{S}_3$ -2D islands displaced by the STM tip under standard imaging conditions. Abrupt horizontal island cuts indicate displacement. The STM tip induced shift of both types of islands demonstrates their weak coupling to the substrate. Image information: (a,b) size $60\text{ nm} \times 60\text{ nm}$, $V_s = 1.0\text{ V}$, $I_t = 0.2\text{ nA}$.

Supplementary Note 3: LEED of the $\sqrt{3} \times \sqrt{3}$ - phase

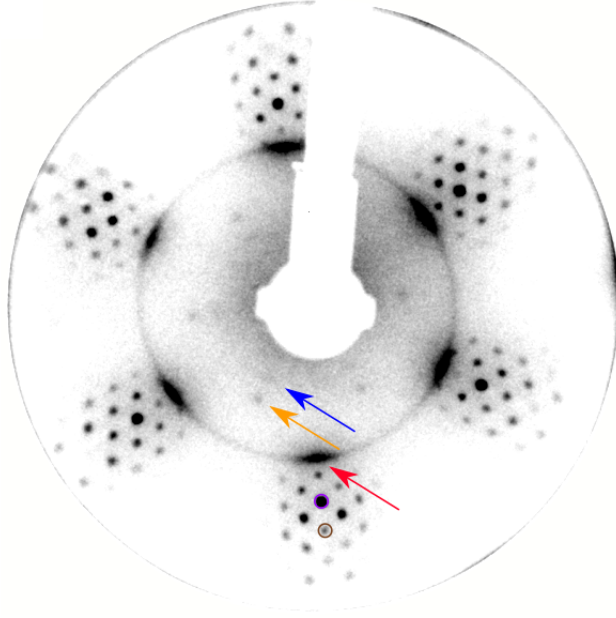


Figure S3: Inverted 140 eV LEED pattern of the $\sqrt{3} \times \sqrt{3}$ - phase obtained after annealing NbS₂ to 1020 K. First order reflections of Ir and Gr are marked with magenta and brown circles, respectively. A fundamental spot of the $\sqrt{3} \times \sqrt{3}$ - phase is marked by a red arrow. Two sets of $\sqrt{3} \times \sqrt{3}$ R30° superstructure spots are observed. One is with respect to Ir and due to S intercalated between Ir(111) and Gr (green). The other set is with respect to the fundamental $\sqrt{3} \times \sqrt{3}$ - phase reflection (orange).

Supplementary Note 4: S 2p components and total S 2p core level intensity as a function of temperature during NbS₂ transformation by annealing.

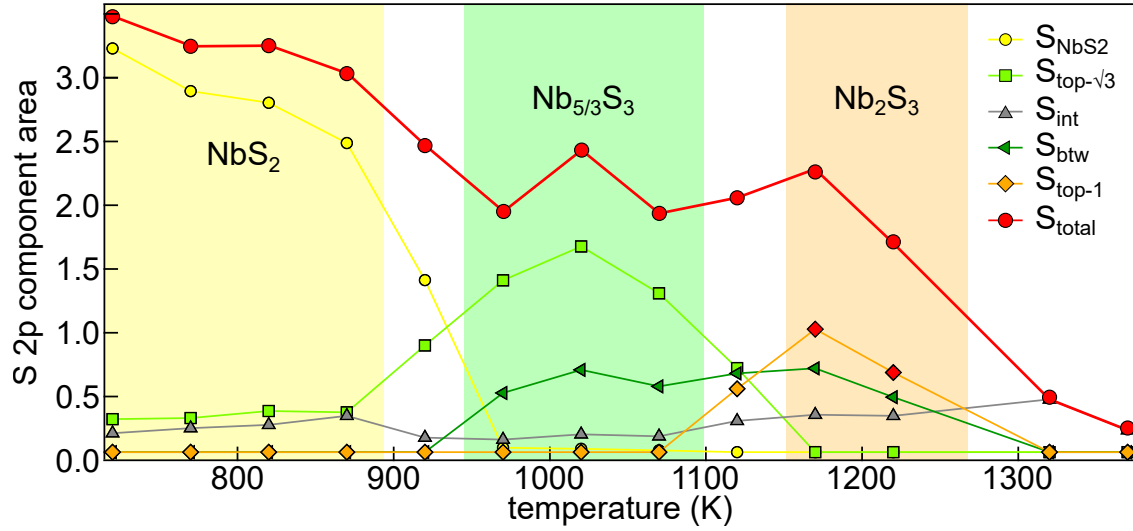


Figure S4: Integrated intensities of the fit components (as in Figure 4b,c,d in the main text) as a function of temperature. Total S 2p intensity in red. The background is color coded according to the dominating S 2p component: yellow (NbS₂), green ($\sqrt{3} \times \sqrt{3}$ - phase), and orange (1×1 - phase).

Supplementary Note 5: Nb 3d, C 1s, and Ir 4f core-levels as a function of temperature during NbS₂ transformation by annealing.

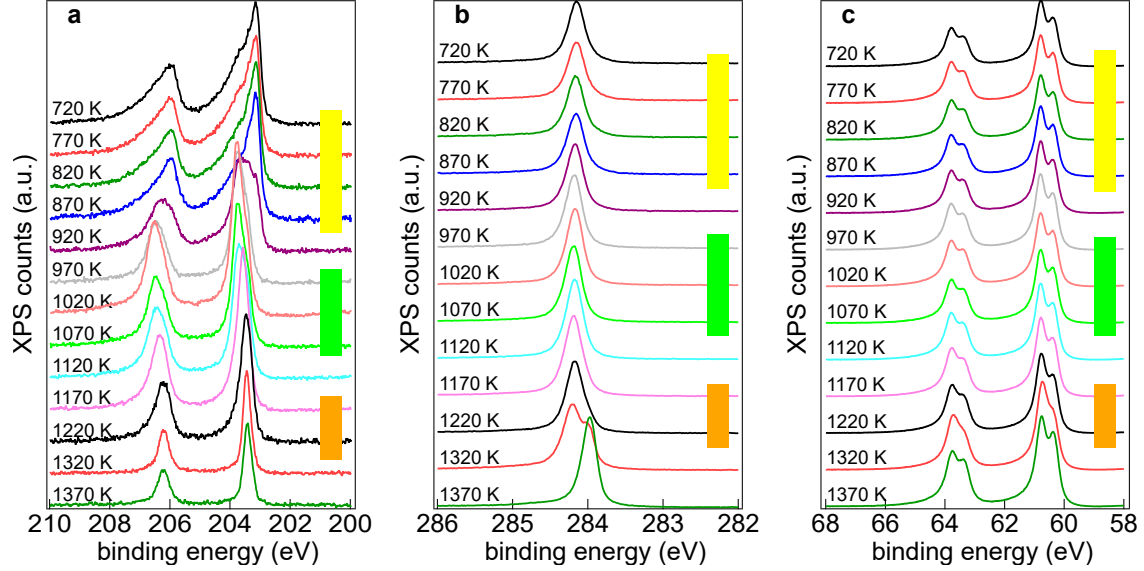
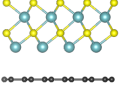
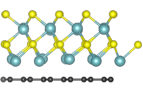
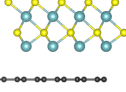
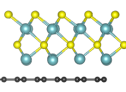
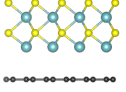
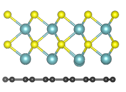


Figure S5: (a) High-resolution X-ray photoemission spectroscopy of the Nb 3d, C 1s, and Ir 4f core levels during NbS₂ transformation by annealing from 720 K to 1370 K. Each data point was measured at room temperature after annealing to the indicated temperature without supply of addition S. Three temperature ranges are grouped according to the features identified in the S 2p core level from Figure 4a in the main text. The groups are color coded accordingly: yellow, green, and orange. Photon energies: $h\nu = 300$ eV for Nb 3d, $h\nu = 380$ eV for C 1s, and $h\nu = 150$ eV for Ir 4f.

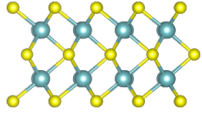
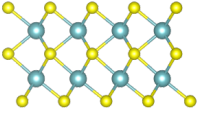
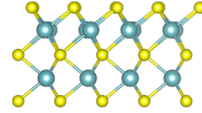
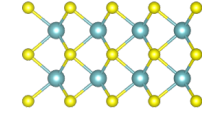
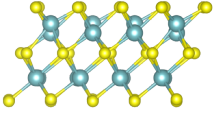
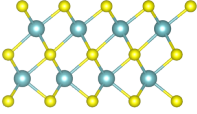
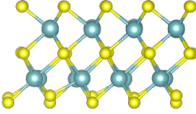
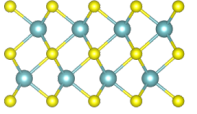
Supplementary Note 6: DFT calculated Nb₂S₂-2D structures on Gr

Table S1: DFT calculated Nb₂S₂-2D structures on Gr. Nb coordination is either trigonal prismatic (H) or octahedral (T)

Nb coordination	1H	1H	1T	1T	1H	1H
Nb-Nb position	shifted	shifted	aligned	aligned	aligned	aligned
structure						
ΔE (eV/Nb ₂ S ₂)	1.552	0.719	0.952	0.198	0.766	0.0000
Nb-C bond	phys	chem	phys	chem	phys	chem
height (nm)	0.827	0.702	0.833	0.699	0.826	0.699
trimerization	1×1	yes	1×1	yes	1×1	1×1

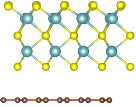
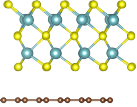
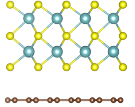
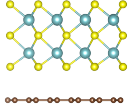
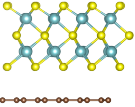
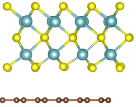
Supplementary Note 7: DFT calculated Nb₂S₃-2D structures on Gr

Table S2: DFT calculated Nb₂S₃-2D structures on Gr for all possible stacking sequences. Nb coordination is either trigonal prismatic (H) or octahedral (T)

coordination	1T/1T	1H/1T	1T/1H	1H/1H
Nb-Nb position	aligned	aligned	aligned	aligned
structure				
ΔE (eV/Nb ₂ S ₃)	0.4538	0.3049	0.2634	0.0000
height (nm)	0.975	0.975	0.975	0.976
trimerization	yes	1 × 1	yes	1 × 1
coordination	1T/1T	1T/1H	1H/1T	1H/1H
Nb-Nb position	shifted	shifted	shifted	shifted
structure				
ΔE (eV/Nb ₂ S ₃)	1.3786	1.0962	1.0517	0.6858
height (nm)	0.977	0.984	0.983	0.984
trimerization	yes	1 × 1	yes	1 × 1

Supplementary Note 8: DFT calculated Nb_{5/3}S₃-2D structures on Gr

Table S3: Calculated Nb_{5/3}S₃-2D structures on Gr. Nb coordination is either trigonal prismatic (H) or octahedral (T)

coordination	1T/1H		1H/1H		1T/1T	
Nb-Nb position	aligned		aligned		aligned	
1/3 Nb missing	top	bottom	top	bottom	top	bottom
structure						
height (nm)	0.964	0.970	0.968	0.972	0.958	0.954
ΔE (eV/Nb _{5/3} S ₃)	0.0000	0.6011	0.2378	0.2505	0.3736	0.3698